Electronic Supplementary Material (ESI) for Journal of Materials Chemistry A.

ENHANCED STABILITY OF PEROVSKITE-LIKE $SrVO_3$-BASED ANODE MATERIALS BY DONOR-TYPE SUBSTITUTIONS

Javier Macías, Aleksey A. Yaremchenko *, Jorge R. Frade

CICECO – Aveiro Institute of Materials, Department of Materials and Ceramic Engineering,

University of Aveiro, 3810-193 Aveiro, Portugal

** Corresponding author. Fax: +351-234-370204; Tel: +351-234-370235; E-mail: ayaremchenko@ua.pt*

Electronic supplementary information

Table S1

Literature data on solid solution formation ranges in pseudo-binary $Sr_{1-x}La_xVO_{3-\delta}$ system

Reported compositional range	Crystal lattice	Ref.
$0.6 \le x \le 1.0$	hexagonal (rhombohedral)	[1]
$x < 0.6$	multiphase	[2]
$0.60 \le x < 0.77$	rhombohedral $LaCoO_3$-type	
$0.77 \le x < 1.0$	orthorhombic $GdFeO_3$-type	
$x < 0.8$	cubic	[3]
$0.8 \le x \le 1.0$	tetragonal	
$0.1 \le x < 0.7$	cubic perovskite *	[4]
$0.7 \le x \le 1.0$	tetragonal perovskite	
$0.5 \le x \le 0.8$	cubic perovskite	[5]
$0.5 \le x \le 0.7$	rhombohedral	[6]
$0.8 \le x \le 1.0$	pseudotetragonal	
$x = 0.7, 0.8$	cubic perovskite	[7]
$x = 0.3, 0.5, 0.7$	cubic perovskite **	[8,9]
$x < 0.5$	multiphase	[10]
$x = 0.5$	cubic perovskite ***	
$0.6 \le x \le 0.8$	multiphase	
$0.9 \le x \le 1.0$	orthorhombic perovskite	

* phase purity or lattice symmetry is not certain for some samples.
** broadened XRD peaks; phase purity is not certain.
*** phase purity is not certain.

[1] P. Dougier and A. Casalot, *J. Solid State Chem.*, 1970, **2**, 396–403.
[2] P. Dougier and P. Hagenmuller, *J. Solid State Chem.*, 1975, **15**, 158–166.
[3] T. Shin-ike, T. Sakai, G. Adachi and J. Shiokawa, *Mater. Res. Bull.*, 1976, **11**, 249–254.
[4] A. V. Mahajan, D. C. Johnston, D. R. Torgeson and F. Borsa, *Phys. Rev. B*, 1992, **46**, 10973–10985.
[5] V. V. Skopenko, S. A. Nedilko, T. P. Lishko and V. A. Drozd, *Dokl. Akad. Nauk Ukr. SSR*, 1993, No.10, 150–152.
[6] F. Inaba, T. Arima, T. Ishikawa, T. Katsufuji and Y. Tokura, *Phys. Rev. B*, 1995, **52**, R2221–R2224.
[7] S. Hui and A. Petric, *Solid State Ionics*, 2001, **143**, 275–283.
[8] Z. Cheng, S. Zha, L. Aguilar and M. Liu, *Solid State Ionics*, 2005, **176**, 1921–1928.
[9] K.-Z. Fung, S.-Y. Tsai and C.-Y. Liu, *ECS Trans.*, 2013, **57**, 1423–1428.
[10] X. M. Ge and S. H. Chan, *J. Electrochem. Soc.*, 2009, **156**, B386.

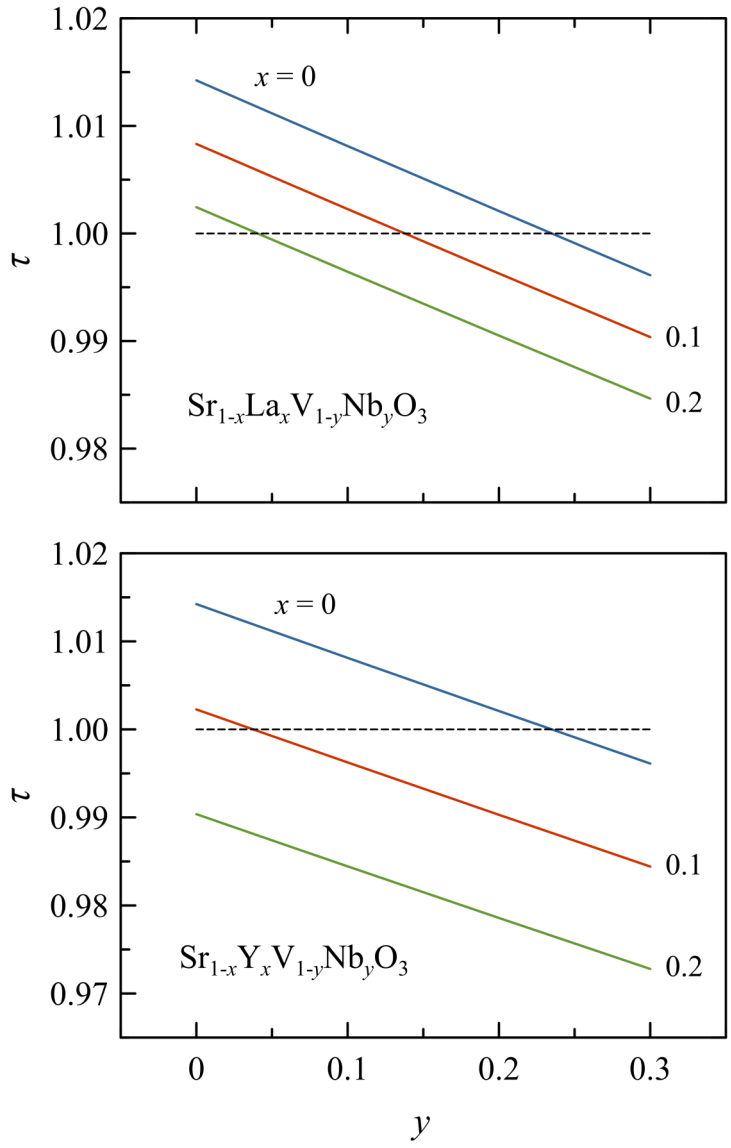

Figure S1. Calculated Goldschmidt tolerance factors for $Sr_{1-x}Ln_xV_{1-y}Nb_yO_3$: Ln = La (top) and Ln = Y (bottom).

Notes:

1) Tolerance factors are calculated using Shannon's radii Ref. [11].

2) Ionic radius of Y^{3+}(CN = 12) was estimated based on the standard 11% increase from nine-coordinate radii for other rare-earth ions, as suggested in Ref.[12].

[11] R. D. Shannon, *Acta Crystallogr. Sect. A*, 1976, **32**, 751–767.

[12] C. Eylem, G. Saghi-Szabo, B. H. Chen, B. Eichhorn, J. L. Peng, R. Greene, L. Salamanca-Riba and S. Nahm, *Chem. Mater.*, 1992, **4**, 1038–1046.

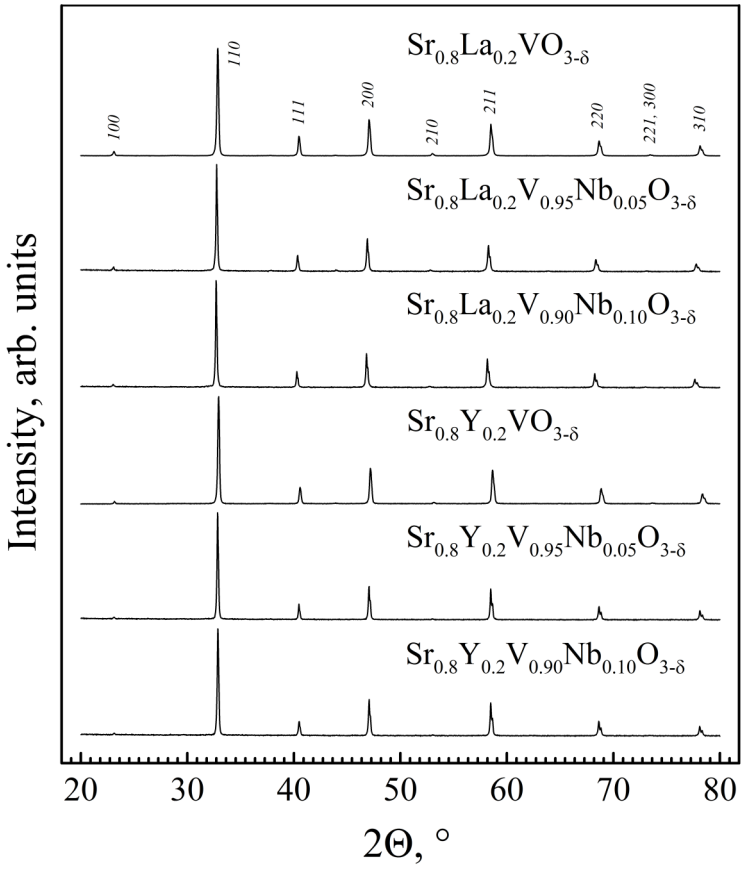

Figure S2. XRD patterns of as-prepared $Sr_{0.8}Ln_{0.2}V_{1-y}Nb_yO_{3-\delta}$ ceramics.

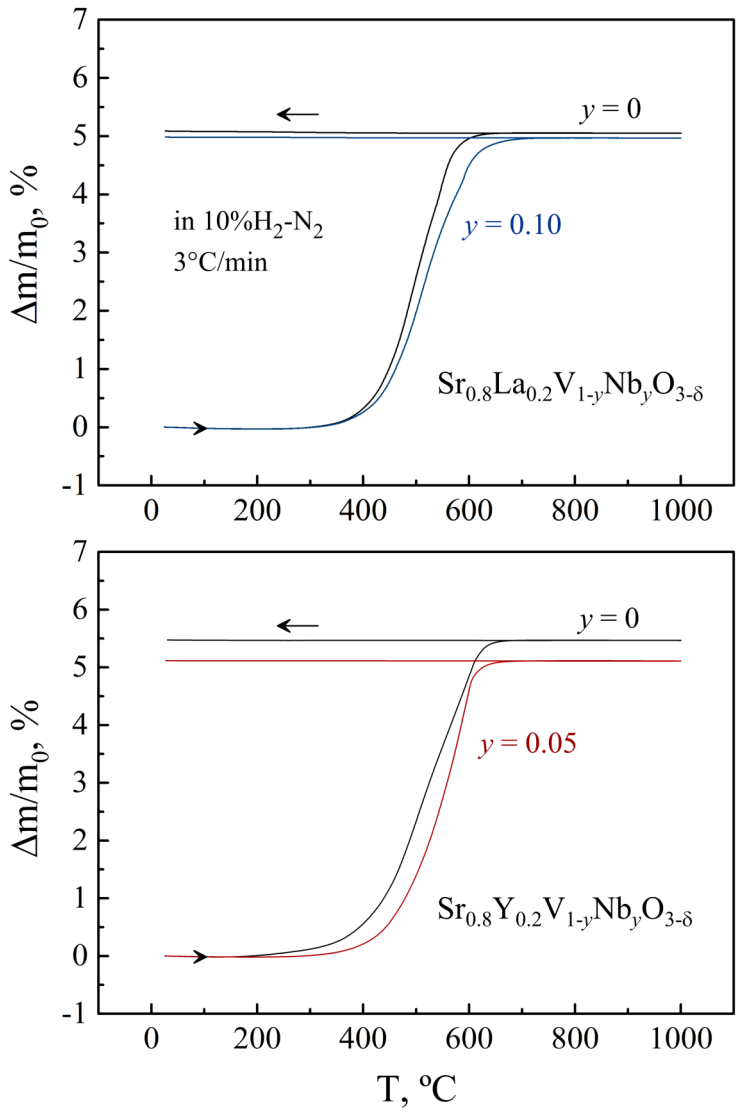

Figure S3. Relative weight gain on oxidation of powdered $Sr_{0.8}Ln_{0.2}V_{1-y}Nb_yO_{3-\delta}$ ceramic samples in one heating/cooling cycle in air.

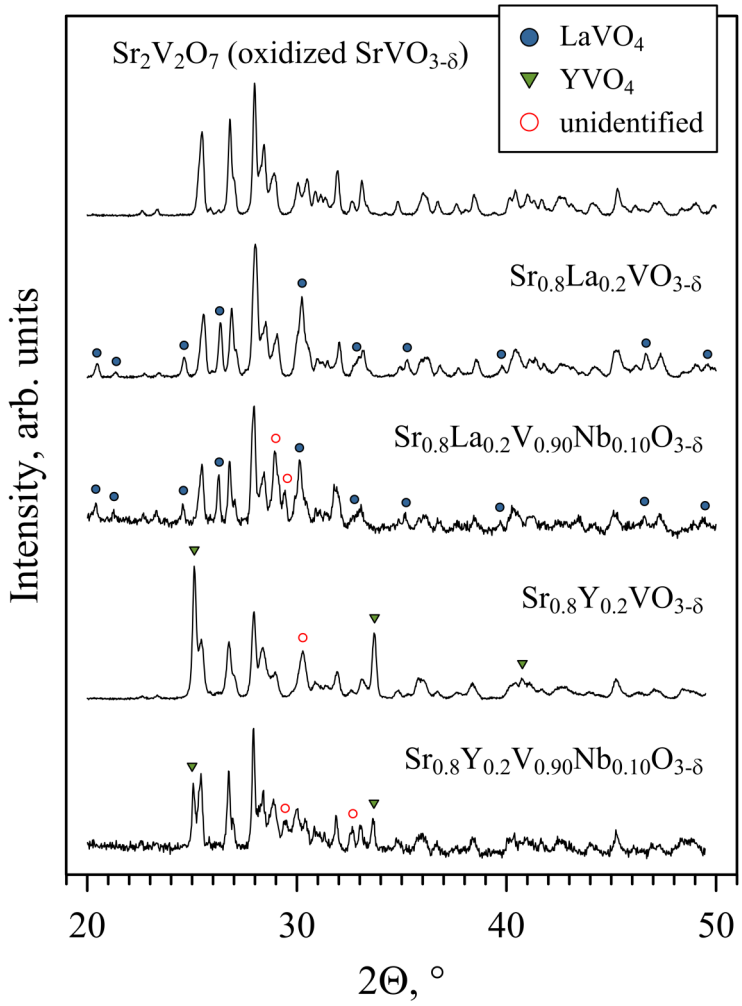

Figure S4. XRD patterns of $Sr_{1-x}Ln_xV_{1-y}Nb_yO_{3-\delta}$ oxidized in air in one heating/cooling cycle (2°C/min, T_{max} = 1000°C). Most intense reflections of $LaVO_4$ (JCPDS PDF # 75-3158), YVO_4 (JCPDS PDF # 82-1968) and unidentified phase(s) are marked with symbols. Unmarked intense reflections belong to $Sr_2V_2O_7$ phase (JCPDS PDF # 81-0737).

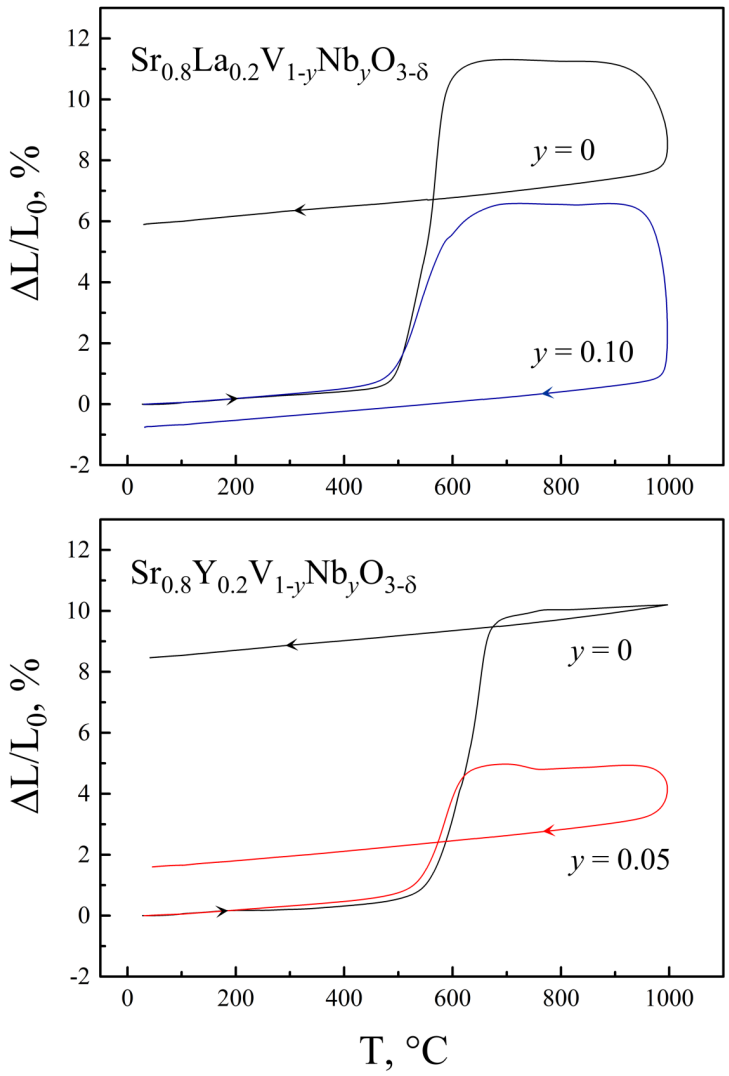

Figure S5. Relative length change of $Sr_{0.8}Ln_{0.2}V_{1-y}Nb_yO_{3-\delta}$ ceramic samples on oxidation in one heating/cooling cycle (3°C/min) in air.

Oxidation in air is accompanied with significant dimensional changes as confirmed by dilatometry (Fig.S5). Significant expansion at 500-700°C originating mainly from $SrVO_3 \rightarrow Sr_2V_2O_7$ phase transformation is followed sometimes with some contraction at temperatures close to 1000°C (maximum T used in this work). This occurs due to the plastic deformation of samples under non-zero mechanical load in dilatometric equipment, possibly caused by formation of intermediate phases with low melting point, such as $Sr(VO_3)_2$ (T_{melt} = 645-690°C) or V_2O_5 (T_{melt} = 681°C). The deformation results in a length contraction of bar-shaped ceramic samples accompanied however with expansion of cross-sectional area, overall volume increase, and reduction of porosity. Qualitatively, deformation of samples is not completely reproducible (Fig.S6), probably due to slightly different initial dimensions and mechanical load (not controllable in the present case), but the shape of dilatometric curves remains the same. Table S2 compares the dimensional changes for two $Sr_{0.8}La_{0.2}V_{0.90}Nb_{0.10}O_{3-\delta}$ ceramic samples after dilatometric measurements up to 750°C and 1000°C, and Fig.S7 illustrates the corresponding evolution of microstructure.

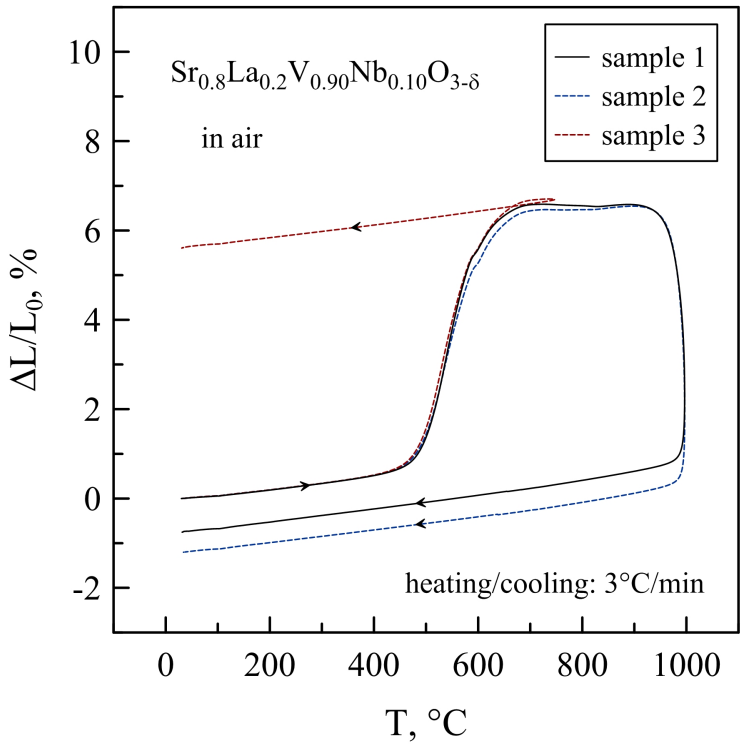

Figure S6. Reproducibility of relative length changes of $Sr_{0.8}La_{0.2}V_{0.90}Nb_{0.10}O_{3-\delta}$ ceramics on heating in air. Samples 1 and 2 were heated to 1000°C, and sample 3 – to 750°C.

Table S2

Dimensional changes of $Sr_{0.8}La_{0.2}V_{0.90}Nb_{0.10}O_{3-\delta}$ ceramics after dilatometric studies (see Figure S6)

Sample 2 (T_{max} = 1000°C)	Sample 3 (T_{max} = 750°C)
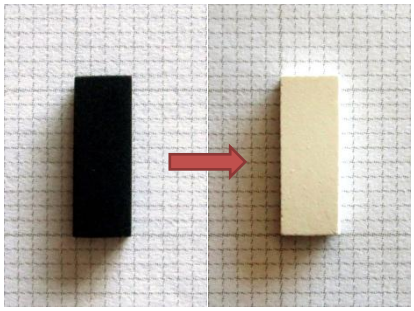	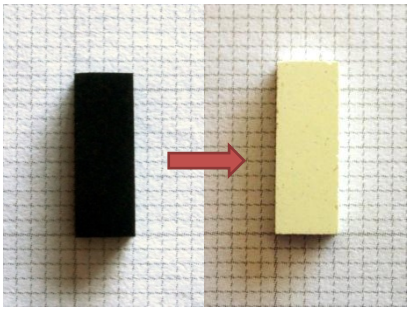

after experiment:

	ΔL, %	ΔS, %	ΔV, %	Density, g/cm^3
Sample 2	-1.2	8.7	7.4	3.10
Sample 3	5.6	12.2	18.5	2.94

Note: L, S and V are the bar-shaped sample length, cross-section area and volume, respectively

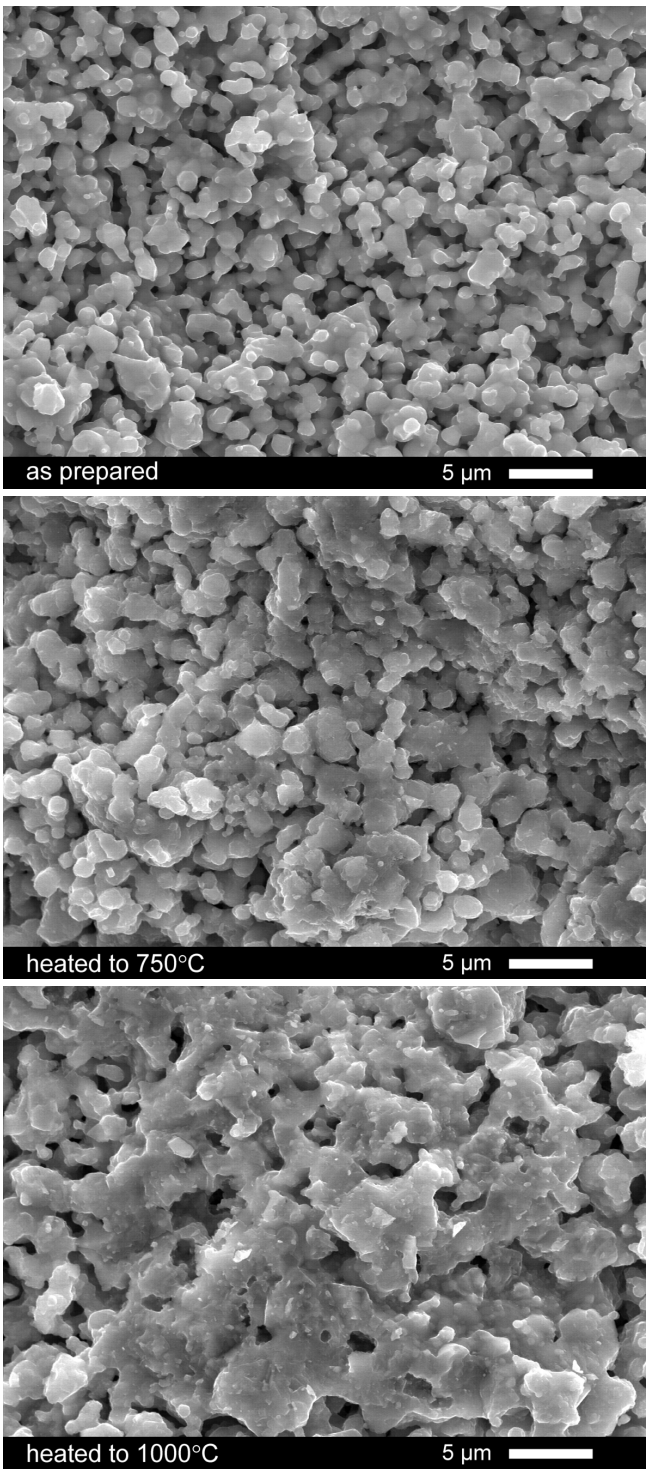

Figure S7. Comparison of microstructure of $Sr_{0.8}La_{0.2}V_{0.90}Nb_{0.10}O_{3-\delta}$ ceramics: as-prepared (top) and after dilatometric studies in air at 25-750°C (middle, sample 3) and at 25-1000°C (bottom, sample 2).

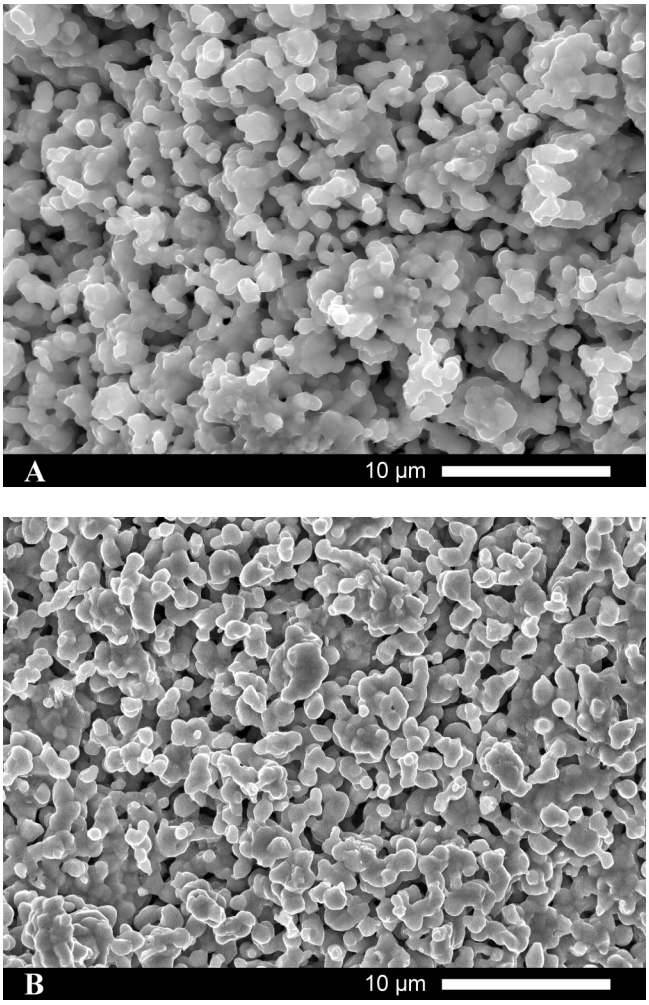

Figure S8. SEM micrographs of fractured $Sr_{0.8}La_{0.2}V_{0.90}Nb_{0.10}O_{3-\delta}$ ceramics: (A) as-prepared and (B) after conductivity relaxation studies in one 10% $H_2 \rightarrow Ar \rightarrow 10\%H_2$ redox cycle at 900°C.

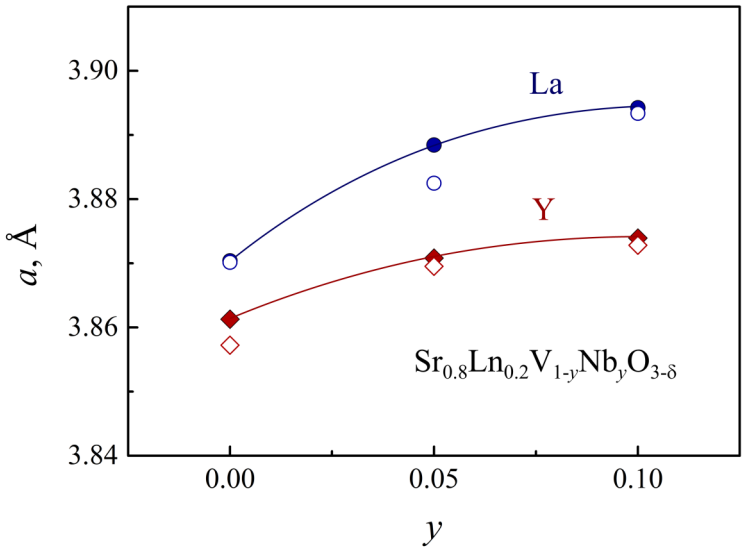

Figure S9. Comparison of the lattice parameters of perovskite-type $Sr_{0.8}Ln_{0.2}V_{1-y}Nb_yO_{3-\delta}$: as-prepared (closed symbols) and after heating-cooling cycle (T_{max} = 1200°C) in argon flow (open symbols).

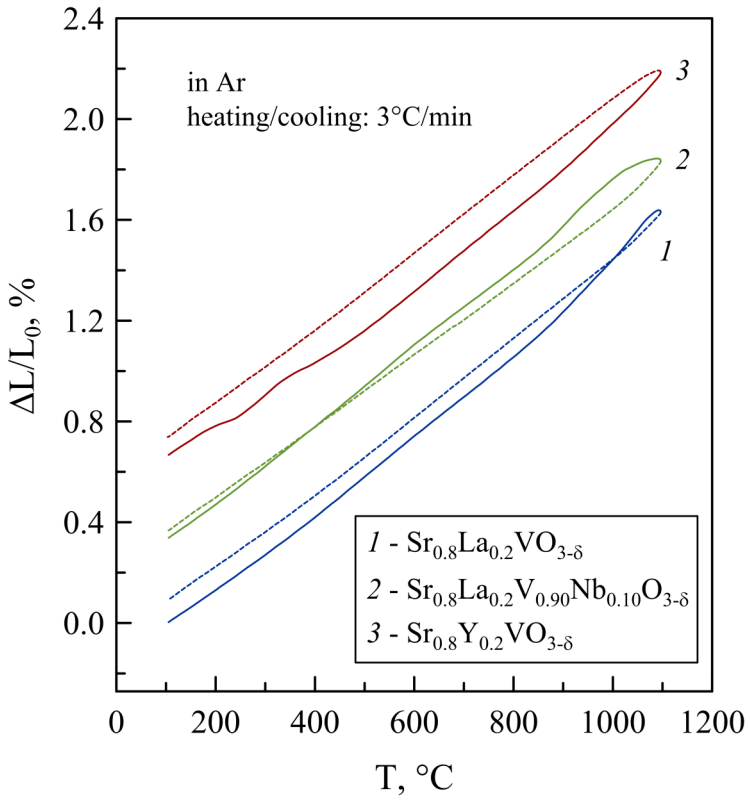

Figure S10. Dilatometric curves of $Sr_{0.8}Ln_{0.2}V_{1-y}Nb_yO_{3-\delta}$ ceramics on heating (solid lines) and subsequent cooling (dotted lines) in argon flow. The curves are shifted with respect to each along Y axis for clarity.

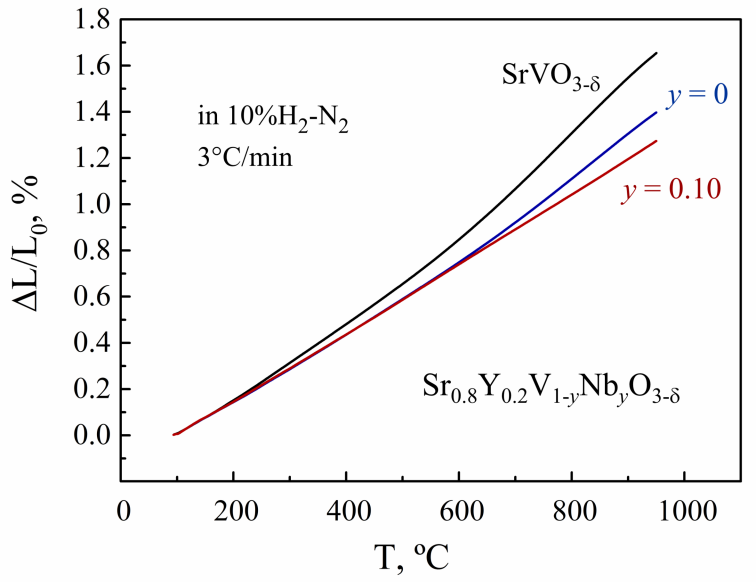

Figure S11. Dilatometric curves of $Sr_{1-x}Y_xV_{1-y}Nb_yO_{3-\delta}$ ceramics in $10\%H_2$-N_2 atmosphere.